NRC Publications Archive
Archives des publications du CNRC

Omega-phase in Ti-Hf-Zr alloys produced by the hydride-cycle method

Swainson, Ian P.; Dolukanyan, Seda K.; Aleksanyan, Anahit G.; Shekhtman, Veniamin Sh.; Mayilyan, Davit G.; Yonkeu, André L.

NRC Publications Record / Notice d'Archives des publications de CNRC:
https://nrc-publications.canada.ca/eng/view/object/?id=131b415a-a84d-48b7-a759-6873a127ba6l
https://publications-cnrc.canada.ca/fra/voir/objet/?id=131b415a-a84d-48b7-a759-6873a127ba6b

Questions? Contact the NRC Publications Archive team at
PublicationsArchive-ArchivesPublications@nrc-cnrc.gc.ca. If you wish to email the authors directly, please see the first page of the publication for their contact information.

Vous avez des questions? Nous pouvons vous aider. Pour communiquer directement avec un auteur, consultez la première page de la revue dans laquelle son article a été publié afin de trouver ses coordonnées. Si vous n'arrivez pas à les repérer, communiquez avec nous à PublicationsArchive-ArchivesPublications@nrc-cnrc.gc.ca.

National Research Council Canada   Conseil national de recherches Canada

Canada

Omega-phase in Ti-Hf-Zr alloys produced by the hydride-cycle method[1]

**Ian P. Swainson, Seda K. Dolukanyan, Anahit G. Aleksanyan,
Veniamin Sh. Shekhtman, Davit G. Mayilyan, and André L. Yonkeu**

Abstract: We report the presence of large proportions of ω-phase in Ti-Hf-Zr alloys, prepared using the hydride cycle technique. We show that the ω-phase extends across the concentration triangle of Ti-Zr-Hf and report the partitioning of the three metals across the two sites in this structure from neutron and X-ray data. We examine the symmetry of the order parameter governing the β–ω phase transition and show that a two-step model for the phase transition involving site ordering followed by displacement is not likely to be correct. We suggest that an interstitial solid solution of oxygen and octahedral vacancies exists, and that the observation of any ω-phase diffraction pattern of alloys of these metals at ambient temperature and pressure should be viewed as a potential sign of the presence of oxygen in the octahedral interstitial sites.

PACS Nos: 72.80.Ga, 61.05.F-, 61.66.Bi, 81.30.Bx

Résumé : Dans cet article, nous rapportons la présence d'une importante proportion de la phase dite ω dans les alliages Ti-Hf-Zr, préparés par une technique de cyclage sous hydrogène (hydride cycle). Nous montrons également que la phase ω s'étend à travers le diagramme de concentration triangulaire de Ti-Hf-Zr. De plus, à partir de données de diffractions des neutrons, nous trouvons que les trois métaux se répartissent sur les deux sites distincts dans la structure. Nous examinons la symetrie du paramètre d'ordre qui gouverne la transition de phase β-ω et nous montrons qu'un modèle à deux étages pour la transition de phase est improbable. Nous suggérons plutôt la présence d'une solution solide interstitielle d'oxygène et de lacunes octaédriques. De plus, si la phase ω est observée dans le diagramme de diffraction d'alliages de ces métaux à température et pression ambiante, on doit la considérer comme un signe possible de la présence d'oxygène sur les sites interstitiels octaédriques.

1. Introduction

A new method of synthesizing alloys via the hydride cycle of self-propagating high-temperature synthesis (SHS), using the hydrides of refractory metals as starting materials, has been recently developed at the Institute of Chemical Physics, Armenian National Academy of Sciences [1]. Detailed descriptions of the conditions of alloy formation from their corresponding metal hydrides have been presented previously, together with the influence of process parameters, including composition of initial hydrides and phase transformations during dehydrogenation [1]. Upon heating of the compacted mixture of hydrides, e.g., $x\text{TiH}_2 + (1 - x)\text{ZrH}_2$, a

I.P. Swainson[2] and A.L. Yonkeu.[3] Canadian Neutron Beam Centre, National Research Council of Canada, Chalk River Laboratories, Chalk River, ON K0J 1J0, Canada.
S.K. Dolukanyan, A.G. Aleksanyan, and D.G. Mayilyan. Institute of Chemical Physics, Armenian National Academy of Sciences, 5/2 P. Sevak Str, Yerevan 0044, Armenia.
V.Sh. Shekhtman. Institute of Solid State Physics, Russian Academy of Sciences, Chernogolovka, Moscow District, 142432, Russia.

[1]Special issue on Neutron Scattering in Canada.
[2]Corresponding author (e-mail: Ian.Swainson@nrc.gc.ca).
[3]Present address: Radiological Protection Research and Instrumentation, Atomic Energy of Canada Limited, Chalk River Laboratories, Chalk River, ON K0J 1J0, Canada.

strong activation of the metals occurs at a temperature slightly higher than that of the dissociation of the hydride [1–5]. Using this method, the temperature necessary for the formation of alloys is typically 600–800 °C lower than that by induction (or arc) fusion or by diffusion sintering. If desired, the new alloy may be rehydrided, as the alloys may have quite different hydrogen absorption capacity than those of its constituent elements.

The drive behind this study was to make hydrides for neutron shielding. Absorption cross-sections are generally strongly energy dependent, being much larger in the thermal regime. Therefore, traditional neutron shielding are composites consisting of thicknesses of H-rich materials, such as polyethelene, and a final barrier of materials with large absorption cross-sections for thermal neutrons, such as Cd, B, and Gd. Metal hydrides are natural composite shielding materials: (*i*) they have a high concentration of ^{1}H with its large, dominantly incoherent, scattering cross-section, which attenuates neutron beams, (*ii*) the light mass of ^{1}H, together with (*i*), makes hydrides a very effective moderator of fast neutrons, and (*iii*) hydrides containing metals such as Hf, with high absorption cross-sections for thermal neutrons, makes them very attractive shielding materials. For most metal hydrides, the path length required to moderate a 2 MeV neutron to a 0.1 eV neutron is 2–4 cm, and the mean free path of a thermalized neutron is typically <2 mm [6].

The main opposition to using metal hydrides as shielding materials would be a risk of fire. Finely divided powders of Zr, Hf, and Ti were used as starting materials and are known to be oxidized; use of such passivated materials has the ad-

Fig. 1. Concentration triangle for Ti-Zr-Hf. The shaded band (Region 2) is the region in which α- and ω-phases were observed. The white bands (Regions 1 and 3) are the areas in which only α was observed by X-ray diffraction.

vantage that the final products are much less likely to be pyrophoric, and therefore more likely to be acceptable for shielding applications. Sintered HfH_2, which would be an ideal shielding material, proved to be mechanically unstable in pellet form, whereas hydrides of Ti-Zr-Hf alloys were more stable. Preliminary X-ray studies of a number of these alloys revealed that they crystallized in the α- and ω-phases. The α-phase was expected as it is the thermodynamically stable, hexagonally close-packed (hcp) form. Furthermore, it was found that upon further cycles of hydriding and dehydriding, the α- and ω-phases returned. It is the unusual results from this component of the study we report here.

There are two aims to this study. The first is to determine the origin of the unusual presence, up to 90 wt% for some samples, of the ω-phase in these samples. The second is to put the observations into context, by giving a brief review regarding the ω-phase in analogous alloys and describing what has been reported about the corresponding ω-oxide in the Ti-Zr system. The mechanism of site ordering in Ti-Zr is discussed, in light of a symmetry analysis of the phase transition. This symmetry analysis is also used to show that the derivative ω'-oxide structure listed in the ICSD is incorrect. We will use the term ω-phase to refer to both ω-alloy and ω-oxide and will only use the latter terms where we need to be specific.

2. Experimental

The samples were prepared by the hydride cycle method [1]. TiH_2 (H content 4.01 wt%), ZrH_2 (H content 2.16 wt%), and HfH_2 (H content 1.09 wt%), initially created by SHS from powdered Zr, Ti, and Hf, were produced [7–9]. The synthesis of alloys and hydrides of the Ti-Zr system using these methods has been previously reported [1–3]. The hydride pellets were crushed, mixed, re-compacted under pressure, and finally dehydrogenated by vacuum annealing

at temperatures up to 1050 °C, providing active dissociation of the hydrides yielding alloys: e.g., $x TiH_2 + (1 - x)ZrH_2 \rightarrow Ti_x Zr_{(1-x)} + H_2 \uparrow$. To characterize the samples, chemical, DTA (Derivatograph Q-1500), and a Siemens D-500 X-ray powder diffractometer were used.

Using the hydride cycle, binary and ternary alloys with α- and ω-phases were produced in the Ti-Zr-Hf system. As the initial project was to prepare neutron absorbers for shielding, most of the alloys produced contained Hf and were not ideal for neutron diffraction. Therefore, we concentrated on two samples with large proportions of ω along the Ti-Zr tie line for neutron diffraction analysis — TiZr and Ti_2Zr — along with two Hf-poor ternaries for detailed study on the C2 neutron powder diffractometer on the NRU reactor, Chalk River, Ontario.

3. Results

3.1 Precursor materials

X-ray and neutron diffraction data were taken of the Zr, Ti, ZrD_2, and TiD_2 starting powders. α-ZrO_2 (badellyite) was found in the Zr and in the ZrD_2 powder, in which we estimated Zr:O:D::1:0.1:1.9 from the phase assemblage. No free oxide was found on the Ti, but there is a high degree of solubility of O in the octahedral interstices of the α- and β-phases of these metals and even the (oxy)hydrides [10–12]. As H typically is found in the tetrahedral interstices of metals, there is usually not direct competition for sites with O.

3.2 The ω-phase

Figure 1 shows a ternary diagram for Ti-Zr-Hf on which the compositions of various samples produced by the hydride cycle are plotted. In the lighter bands (Regions 1 and 3), only α-phase was detected by X-rays. The shaded band, Region 2, is that in which α- and ω-phases were found to coexist at room temperature. It is possible that small amounts of ω-phase exist in Regions 1 and 3 also, but if so, they are below the detection limit of the X-ray measurements, which means that the ω fraction would be below a few percent. The Ti-Hf tie line has been studied before but never the entire Ti-Zr-Hf compositional space [13]. There is a coexistence along the two binaries, Ti-Zr (in agreement with [14]) and Ti-Hf, but not along Hf-Zr. Attempts were made to form such Hf-Zr ω-phases by varying the temperature of dehydrogenation, but they were not successful.

In high-purity Ti and Zr, the ω-phase appears as the thermodynamically stable phase at $P > 40$–70 kbar (1 bar = 100 kPa) [15–17]. The relationship to the bcc β-phase of such metals is simple and can be viewed as a displacive mechanism. A dip in the longitudinal acoustic (LA) phonon dispersion of all bcc metals in this group exists near wavevector $\boldsymbol{k}$ = (2/3, 2/3, 2/3), showing an incipient instability of the bcc lattice with respect to the ω-phase [18–21]. The soft LA mode is associated with a collapse of {222} planes of the bcc lattice. If the collapse is "complete", i.e., atoms in both collapsing layers lie at $z = 1/2$ in the new lattice, the symmetry is hexagonal, $P6/mmm$, and the phase is called the ideal ω-phase; if incomplete, i.e., the collapsing planes of atoms do not quite reach $z = 1/2$, the symmetry is trigonal, $P\bar{3}m1$, and the structure is sometimes termed the intermedi-

Table 1. Possible subgroups of $Im\bar{3}m$ that can be induced by the action of a soft LA mode Λ_1 (labelling of Miller and Love [29]) for wavevector $\boldsymbol{k}_\omega$ = (2/3, 2/3, 2/3). There is no origin shift between parent a subgroup lattices. Left: space group symbol; middle: order parameter direction, describing which components of the 8-dimensional order parameter are involved; right: the basis of the new cell with respect to the $Im\bar{3}m$ unit cell axes.

Space group	Direction	Basis
$P\bar{3}m1$	$(a,0,0,0,0,0,0,0)$	$(1, \bar{1}, 0)$, $(\bar{1}, 0, 1)$, $\left(\frac{\bar{1}}{2}, \frac{1}{2}, \frac{1}{2}\right)$
$Fmmm$	$(a,a,0,0,0,0,0,0)$	$(3, 0, 0)$, $(0, \bar{3}, \bar{3})$, $(0, 1, \bar{1})$
$Im\bar{3}m$	$(a,a,a,0,0,0,0)$	$(0, \bar{3}, 0)$, $(\bar{3}, 0, 0)$, $(0, 0, \bar{3})$
$P\bar{3}m1$	$(a,0,0,0,b,0,0,0)$	$(1, \bar{1}, 0)$, $(\bar{1}, 0, 1)$, $\left(\frac{\bar{1}}{2}, \frac{1}{2}, \frac{1}{2}\right)$
$C2/m$	$(a,b,0,0,0,0,0,0)$	$(0, 3, 3)$, $(0, \bar{1}, 1)$, $\left(\frac{3}{2}, \frac{3}{2}, \frac{3}{2}\right)$
$Fmm2$	$(a,a,0,0,b,-b,0,0)$	$(3, 0, 0)$, $(0, \bar{1}, 1)$, $(0, \bar{3}, \bar{3})$
$Fmm2$	$(a,a,0,0,b,b,0,0)$	$(0, \bar{1}, 1)$, $(0, \bar{3}, \bar{3})$, $(3, 0, 0)$
$I\bar{4}3m$	(a,a,a,a,b,b,b,b)	$(0, \bar{3}, 0)$, $(\bar{3}, 0, 0)$, $(0, 0, \bar{3})$
$R\bar{3}m$	$(a,b,b,b,0,0,0,0)$	$(3, 0, \bar{3})$, $(0, \bar{3}, 3)$, $\left(\frac{3}{2}, \frac{3}{2}, \frac{3}{2}\right)$
$Fmmm$	$(a,b,b,a,0,0,0,0)$	$(0, 0, \bar{3})$, $(3, 3, 0)$, $(3, \bar{3}, 0)$
$I4mm$	$(a,a,a,a,b,-b,-b,b)$	$(3, 0, 0)$, $(0, 3, 0)$, $(0, 0, 3)$
$C2/m$	$(a,b,b,c,0,0,0,0)$	$(0, 0, 3)$, $(3, \bar{3}, 0)$, $\left(\frac{3}{2}, \frac{3}{2}, \frac{3}{2}\right)$
$Fmm2$	$(a,a,b,b,0,0,c,-c)$	$(\bar{3}, 0, 0)$, $(0, 3, 3)$, $(0, 3, \bar{3})$
Cm	$(a,b,0,0,c,d,0,0)$	$(0, 3, 3)$, $(0, \bar{1}, 1)$, $\left(\frac{3}{2}, \frac{3}{2}, \frac{3}{2}\right)$
$R3m$	(a,b,b,b,c,d,d,d)	$(3, 0, \bar{3})$, $(0, \bar{3}, 3)$, $\left(\frac{3}{2}, \frac{3}{2}, \frac{3}{2}\right)$
$Fmm2$	(a,b,b,a,c,d,d,c)	$(\bar{3}, 3, 0)$, $(3, 3, 0)$, $(0, 0, \bar{3})$
$C2$	$(a,b,b,c,0,d,-d,0)$	$(0, 0, 3)$, $(3, \bar{3}, 0)$, $\left(\frac{3}{2}, \frac{3}{2}, \frac{3}{2}\right)$
$P\bar{1}$	$(a,b,c,d,0,0,0,0)$	$\left(\frac{3}{2}, \frac{3}{2}, \frac{3}{2}\right)$, $\left(\frac{3}{2}, \frac{3}{2}, \frac{3}{2}\right)$, $\left(\frac{3}{2}, \frac{3}{2}, \frac{3}{2}\right)$
Cm	$(a,a,b,b,c,-c,d,-d)$	$(0, 3, 3)$, $(3, 0, 0)$, $(0, 0, \bar{3})$
Cm	(a,b,b,c,d,e,e,f)	$(0, 0, 3)$, $(3, \bar{3}, 0)$, $\left(\frac{3}{2}, \frac{3}{2}, \frac{3}{2}\right)$
$P1$	(a,b,c,d,e,f,g,h)	$\left(\frac{3}{2}, \frac{3}{2}, \frac{3}{2}\right)$, $\left(\frac{3}{2}, \frac{3}{2}, \frac{3}{2}\right)$, $\left(\frac{3}{2}, \frac{3}{2}, \frac{3}{2}\right)$

ate ω-phase. We will refer to the structure in both space groups as ω-phase.

3.2.1 The ω-oxide

The presence of the "Ti_2ZrO" ω-oxide is well-established experimentally [13, 14, 22–26], although its existence is not widely appreciated. Domagala et al. reported a study of the pseudobinary Ti-ZrO_2 phase diagram, showed ZrO_2 to be highly soluble in Ti, and reported the existence of a distinct binary oxide [22]. Recently, electron microscopy studies have been made of the ZrO_2–Ti interface reacted at 1550 °C and have shown that α-metal and ω-Ti_2ZrO exist in the reaction field [25, 26]. The first report of the structure of the ω-phase in the Ti-Zr-O system was made by Fykin et al. [23, 24], who suggested the $P6/mmm$ structure as the ω-phase alloy, but with O sitting in an octahedral interstice. Later, Déchamps et al. performed an extensive study on this material [14].

### 3.2.2. Symmetry analysis of the ω-phase

We performed a symmetry analysis to better understand the relationships between the phases and to look at possible mechanisms involved in the transitions. The symmetry programs ISOTROPY and Isodisplacive were used to analyse

the symmetry relations between the phases in this system [27, 28]. As $\boldsymbol{k}_\omega$ = (2/3, 2/3, 2/3), it lies along the Λ-line of the cubic-I Brillouin Zone. As the star of wavevectors, Λ^*, comprises $\{\zeta\zeta\zeta\}$, any order parameter associated with the Λ-line must be at least an 8-dimensional vector. The symmetry of the soft LA mode is Λ_1. Table 1 gives the possible subgroups that can arise in which different components of the Λ_1 order parameter, denoted as Λ_1 $(a, \cdots ,h)$, are involved. Free energy differences would determine which of these possible structures form. The simplest situation is where only one component is involved, which yields $P\bar{3}m1$.

The vast majority of ω-phase refinements have shown that the symmetry is either trigonal $P\bar{3}m1$ or hexagonal $P6/mmm$. Cells other than these have been reported, particularly in the early literature. Domagala et al. [22] and Spachner [30] reported a tetragonal and orthorhombic cell, respectively, but neither is probably correct, as the basis of these cells does not match any in Table 1. Austin and Doig [31] and Lee [32] reported a tripled body-centered cubic cell of symmetry $I\bar{4}3m$, $Im\bar{3}m$, or $I432$, with their <100> axes parallel to those of the parent lattice. The former two cubic cells could be caused by a Λ_1 soft mode (Table 1). However, the atomic displacements associated with the basis vectors that accompany these cells are far more complicated than simple

Fig. 2. Left: Relationship between bcc and the ω-cells. Right top: bcc structure in the intermediate ω-cell showing the two metal sublattice sites (Ti-blue (the light atom in grayscale) in $2d$-sites, Zr-red (the dark atom in grayscale) in $1a$-sites) and the direction of displacement for $+\eta$. Right bottom: The ideal ω-alloy structure where both Ti atoms sit at $z = 1/2$. (Note that displacements in the opposite sense, governed by $-\eta$, would ultimately lead to the anti-ω structure where all Ti, Zr atoms would sit at $z = 0$.)
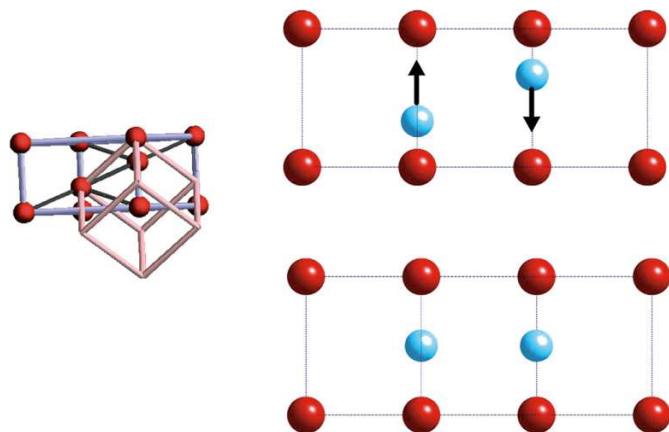
collapses along $< 111 >_{Im\bar{3}m}$; e.g., some metal atoms move along the $< 100 >_{Im\bar{3}m}$ axes. The most probable explanation for observations of tripled-cubic structures is that the 12 variants (domains) of the ω-structure are superimposed into one diffraction pattern giving the appearance of a tripled cubic cell.

Figure 2 shows the relationship between the $Im\bar{3}m$ parent, the trigonal $P\bar{3}m1$, and hexagonal $P6/mmm$, ideal ω structure for a Ti-Zr binary alloy with O in solid solution. The solid solution of Ti and Zr over a single site in the bcc phase is replaced by two distinct metal sites, in which ordering of Ti and Zr can occur. These two metal sites have quite different interatomic distances: Ti prefers the $2d$ sites inside the trigonal–hexagonal unit cells, and Zr the corners (Table 2). The $P6/mmm$ structure is not a subgroup of $Im\bar{3}m$: it cannot be reached by an infinitesimal distortion of the β phase but requires a specific value of displacement of $\sqrt{3}/12$ along the $[111]_{Im\bar{3}m}$ in order that the two atoms lie at the same height along this axis and the symmetry increases to that of the ideal ω-phase. This is an example of a reconstructive transition in which two high-symmetry phases are related displacively via a common low-symmetry intermediate; it is possible to describe this $Im\bar{3}m \rightarrow P6/mmm$ transition in terms of a single transcendental order parameter [33, 34].

The irreducible representation has a Lifshitz invariant, leading to a third-order term in the Landau expansion [35, 36], thus forcing the transition to be discontinuous in nature: this requires a region of coexistence of $\beta + \omega$, which is commonly observed [35–37]. Because of this third-order term, while the order parameters η and $-\eta$ are of the same symmetry, they are inequivalent, ultimately leading to two different structures both with space group $P6/mmm$ of different energies. In both cases Zr atoms sit on nodes, as η and $-\eta$ change the phase of the LA phonon by π: displacements governed by η ultimately generate ideal ω where both Ti lie at $z = 1/2$ (Fig. 2), whereas displacements in the opposite sense, described by $-\eta$, would ultimately lead to the anti-ω-

phase, or h-phase [34], where all Ti and Zr atoms lie at $z = 0$. (The anti-ω-phase provides one possible mapping between ω- and α-phases [33, 34].)

3.2.3 The mechanism of site ordering and displacement

The symmetry-breaking caused by a primary order parameter, η, of a phase transition almost always induces secondary, non-symmetry breaking order parameters; e.g., spontaneous strain is frequently coupled to an atomic displacement. Table 2 shows the order parameters that are generated by a primary Λ_1(a,0,0,0,0,0,0), which we will abbreviate to Λ_1 in the following discussion. Regarding the metal sites, microscopically, this triggers two order parameters that transform as Λ_1, one describing a displacement of atoms and one a site ordering. There is another ordering mode affecting the metal atoms that transforms as the trivial representation Γ_1^+, which, as it is totally symmetric, in practice effects no chemical or site ordering. In addition, the unit cell undergoes a volume strain transforming as another instance of Γ_1^+, and a shear Γ_5^+, describing the change of shape from cubic to trigonal–hexagonal.

β-TiZr alloy is a random solid solution: there is little evidence for significant levels of even short-range order of Ti and Zr in α and β null-scattering TiZr [38]. Dubertret and Fayard proposed a two-step mechanism for the β–ω transition in Ti-Zr alloys, consisting of site ordering of Ti and Zr in $P\bar{3}m1$, followed by a displacement leading to $P6/mmm$ [13]. This appears to be a reasonable physical picture, i.e., that there should be chemical separation onto the two sites, and subsequently large amplitude displacement of the now distinct sites. However, this model seems very unlikely to be correct. The displacive and ordering modes are of identical symmetry, Λ_1, so could both trigger the change of symmetry of the unit cell. However, the representation Λ_1 can couple to itself (Table 2), so that the act of ordering or displacement causes simultaneous action of the other. The only question that can be asked is, which of these two Λ_1 order parameters is the primary that drives the transition. As the ω-phase is known in elemental Ti and Zr, in which such metal site ordering is impossible, it is safe to conclude that it is the displacive Λ_1 order parameter that is the primary. It may seem less physically plausible that the degree of site ordering is a direct function of the displacement of the metal atoms, as demanded by this mechanism. However, there are two reasons why this is not the case: (i) the self-diffusion constants in β-Zr, Ti, and Hf are anomalously high, and this appears to be intimately linked to this soft phonon [18, 39]; (ii) the shear and volume changes in the unit cell are also coupled to (i.e., a function of) the displacement, so that as these effects increase in magnitude the preference of Ti for the $2d$ sites should increase. In addition, as the transition is first order, the displacement and associated site-ordering processes are not continuous.

The hydride cycle involves a dehydrogenation stage at 1000 °C during which the alloys are formed. Any oxygen not already in solid solution but present as oxide films will be dissolved into the alloy, which at the temperatures involved will be in the bcc phase. Oxygen typically lies in the octahedral interstices of bcc metals, so can be expected with partial occupancy on the $\{1/2, 1/2, 0\}$ $6b$ Wyckoff sites. Figure 3 shows the ω-phase displacement and ordering

Table 2. Coordinate mapping between the bcc, the intermediate $P\bar{3}m1$, and ideal $P6/mmm$ ω-phases and the $Cmmm$ ω'-oxide. Below: the local distortion modes of $\beta \to \omega$ transition where the symmetry of the primary order parameter transforms as $\Lambda_1(a,0,0,0,0,0,0,0)$, and the ordering wavevector is $\boldsymbol{k}_\omega = (2/3, 2/3, 2/3)$ (Table 1). The ranges of values of x and z under the column $P\bar{3}m1$ give the limiting values for the structures $Im\bar{3}m$ and $P6/mmm$, δ symbols give displacements, and "occ" lists occupancy changes over the two sites.

$Im\bar{3}m$	$\xrightarrow{\Lambda_1(a,0,0,0,0,0,0,0)}$ $\begin{bmatrix} \bar{\frac{1}{3}} & \frac{2}{3} & \frac{1}{3} \\ \frac{1}{3} & \bar{\frac{1}{3}} & \frac{2}{3} \\ \bar{\frac{1}{3}} & \bar{\frac{1}{3}} & \bar{\frac{2}{3}} \\ \frac{2}{3} & \frac{2}{3} & \frac{2}{3} \end{bmatrix}$	$P\bar{3}m1$	$\xleftarrow{\Gamma_3^+(a)}$ $\begin{bmatrix} 1 & 0 & 0 \\ 0 & 1 & 0 \\ 0 & 0 & 1 \end{bmatrix}$	$P6/mmm$	$\xrightarrow{A_5^+(a)}$ $\begin{bmatrix} 1 & \bar{\frac{1}{2}} & 0 \\ 0 & \frac{1}{2} & 0 \\ 0 & 0 & \frac{1}{2} \end{bmatrix}$	$Cmmm$
TiZr $2a$ $0,0,0$		$1a$ $0,0,0$		$1a$ $0,0,0$ Zr		$2a$ $0,0,0$ Zr $2d$ $0,0,\frac{1}{2}$ Zr
		$2d$ $\frac{1}{3},\frac{2}{3},z$ $z \sim (\frac{1}{3},\frac{1}{2})$		$2d$ $\frac{1}{3},\frac{2}{3},\frac{1}{2}$ Ti		$8n$ $0,-\frac{2}{3},\frac{1}{4}$ Ti
O $6b$ $\frac{1}{2},\frac{1}{2},0$		$3e$ $\frac{1}{2},0,0$		$3f$ $\frac{1}{2},0,0$ O		$\{2b,2c,4f\}$empty $4e$ $\frac{1}{4},\frac{1}{4},0$ O
		$6i$ $x,\bar{x},z$ $z \sim (\frac{1}{3},\frac{1}{2})$ $x \to \frac{5}{6}$		$6m$ $x,\bar{x},\frac{1}{2}$ empty		$\{8n,16r\}$ empty

Microscopic modes for the $Im\bar{3}m \to P\bar{3}m1$ transition. For full description of the distortion mode symbols see [28].

Displacive modes

Distortion mode	atom	δ_x	δ_y	δ_z
$Im\bar{3}m \left[\frac{2}{3},\frac{2}{3},\frac{2}{3}\right] \Lambda_1(a,0,0,0,0,0,0,0)$ [TiZr: a] $T_{1u}(a)$	Zr $1a$	0.0000	0.0000	0.0000
	Ti $2d$	0.0000	0.0000	1.0000
$Im\bar{3}m \left[\frac{2}{3},\frac{2}{3},\frac{2}{3}\right] \Lambda_1(a,0,0,0,0,0,0,0)$ [O: b] $A2_u(a)$	O $3e$	0.0000	0.0000	0.0000
	O $6i$	0.5000	-0.5000	-1.0000
$Im\bar{3}m \left[\frac{2}{3},\frac{2}{3},\frac{2}{3}\right] \Lambda_1(a,0,0,0,0,0,0,0)$ [O: b] $E_u(a)$	O $3e$	0.0000	0.0000	0.0000
	O $6i$	0.2500	-0.2500	1.0000

Occupancy modes

Distortion mode	atom	occ
$Im\bar{3}m \left[\frac{2}{3},\frac{2}{3},\frac{2}{3}\right] \Lambda_1(a,0,0,0,0,0,0,0)$ [TiZr: a]order(a)	Zr $1a$	1.0000
	Ti $2d$	-0.5000
$Im\bar{3}m [0,0,0] \Gamma_1^+(a)$ [TiZr: a]order(a)	Zr $1a$	1.0000
	Ti $2d$	1.0000
$Im\bar{3}m \left[\frac{2}{3},\frac{2}{3},\frac{2}{3}\right] \Lambda_1(a,0,0,0,0,0,0,0)$ [O: b]order(a)	O $3e$	-1.0000
	O $6i$	0.5000
$Im\bar{3}m [0,0,0] \Gamma_1^+(a)$ [O: b]order(a)	Zr $1a$	1.0000
	Zr $2d$	1.0000

Strain

Volume	Shear
$Im\bar{3}m [0,0,0] \Gamma_1^+(a)$	$Im\bar{3}m [0,0,0] \Gamma_5^+(a,a,a)$
$xx+yy+zz$	xy, yz, xz

of both the metal sites (as in Fig. 2) as well as the O sites. As with the metal atoms, Λ_1 displacive modes affect the O atoms, and only the one subset of such sites in $P\bar{3}m1$, $6i$, that does not sit directly on the basal plane of the trigonal cell has nonzero displacement (Table 2). Mapped further into the $P6/mmm$ phase, this becomes the structure of Fykin

[14, 23, 24]. As in the case of the metal sites, there is an ordering mode of symmetry Λ_1 between the two O sublattice sites. In this case, however, it governs the ordering of vacancies, $\square$, and O over the two sites: the observed result is that by the time the structure has evolved to $P6/mmm$, only the $3f$ sites are occupied (Fig. 3 dark green), and the

Fig. 3. Plot of the ω-oxide structures. Zr-red, Ti-blue (at the same positions as in Fig. 2), and two set of O atoms in light and dark green (additional light and dark grays in grayscale). Top: the bcc structure plotted in the ω-cell. Bottom: the *P6/mmm* structure, in which all O has ordered into the 3*f* O sublattice (dark green or gray), where it remains statistically disordered, and the 6*m* sites are empty (light green or gray in the upper part of the figure).
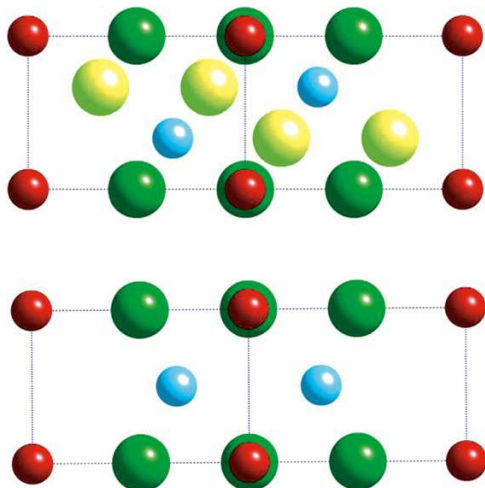
6*m* are vacant (Fig. 3 light green). At this point in its structural evolution, the coordination of 6*m* is no longer octahedral, but hexagonal [40]. For stoichiometric Ti$_2$ZrO, the O sits on the 3*f* site with 1/3 occupancy.

3.2.4. A note on the ω′(O) Cmmm phase

Déchamps et al. reported a further distortion in stoichiometric Ti$_2$ZrO when it is annealed for long periods at low temperature [14]. The resulting lattice is orthorhombic, and the O orders into one of four possible subsites. The relationship between the *P6/mmm* ω-oxide, which they designate ω(O), and the *Cmmm* ordered oxide, designated ω′(O), we found to be described by the representation A_5^+. Our mapping of the Wyckoff sites across the two unit cells agrees with the matrix relationship described by Déchamps; i.e., *f* → {*b*, *e*, *c*, *f*}, of which only *e* is occupied [14]. The description of this structure in the ICSD database (ICSD-9389) is in error as it lists O in the 4*i* sites, which appears to be a transcription error.

3.3. X-ray and neutron diffraction

X-ray diffraction identified the presence of ω-phase at various compositions in the Ti-Zr-Hf concentration triangle. X-ray and neutron powder diffraction measurements of two Ti-Zr samples were made, and refinements on the two datasets were done both together and separately. The background in the neutron powder diffraction patterns is relatively high, especially for Ti$_2$Zr: this composition is nearly that of a null scattering alloy ($\bar{b} = 0$) when Ti and Zr are in solid solution in an unordered structure such as α [38]: $b_{Ti} = -3.37$ and $b_{Zr} = 7.16$ fm [41, 42]. Because of this, the peaks from the α-phase are nearly invisible in the neutron pattern (even though it represents 37 wt%) but very strong in the X-ray pattern (Figs. 4 and 5). On the other hand, because of the very strong scattering contrast between Ti and Zr, preliminary refinements of the neutron data

Fig. 4. Best fit to the X-ray diffraction pattern of alloy Ti$_2$Zr. The observed data points are marked as crosses, and the modelled diffraction pattern is the solid fit to those points. The tick marks underneath the pattern represent peak positions from each phase: the lower set is from the α-phase and the upper set is from the ω-phase. Top: with O in model. Bottom: without O in model.
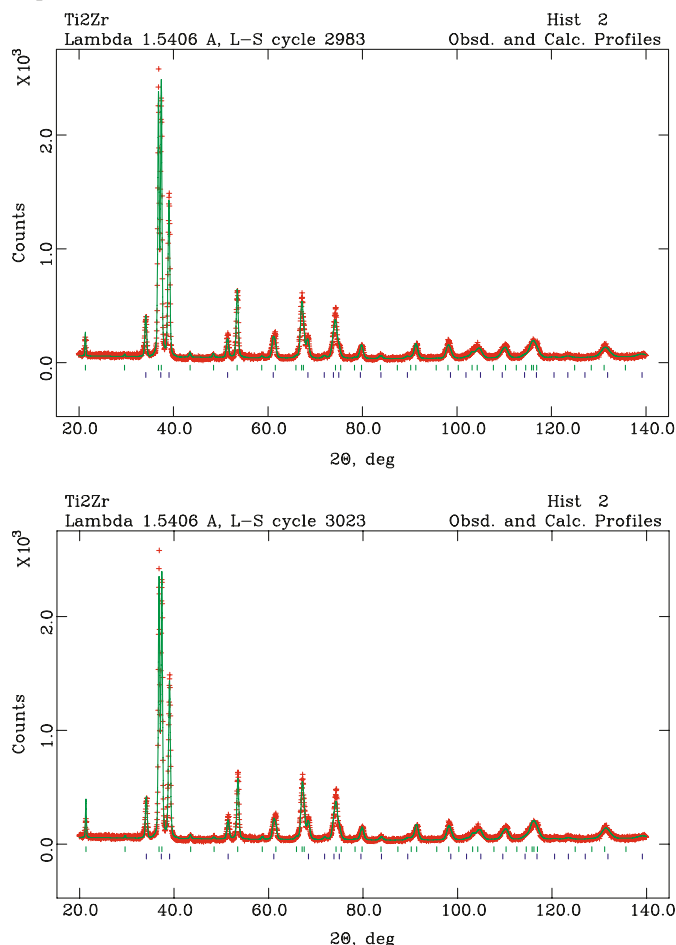

showed very strong site ordering of Ti and Zr over the two metal sites in this structure, in agreement with previous observations of this structure [13, 14, 23, 24]. This pattern is also seen for the two ternary samples studied by X-ray and neutron powder diffraction: a strong preference for the 2*d* site to be Ti-rich and for the 1*a* site to be Zr(Hf)-rich (Table 3).

Whereas the X-ray data of the Ti-Zr samples fitted very well to the published α and ω alloy structures (Fig. 4), all initial attempts to fit the neutron diffraction patterns failed, with strong systematic errors between observed and calculated intensities in ω peaks for (*hkl*), *h*, *k* = 2*n* (Fig. 5). A Fourier difference map showed up a strong residual of positive scattering length sitting at 1/2, 0, 0.

As the symmetry of the ω-oxide and the ω-alloy are identical, no new superlattice peaks are generated, and the difference in structure factors between the ω-alloy and an ω-oxide is very small for X-ray diffraction. Upon introducing an O onto the preferred octahedral site, the differences between the observed and calculated neutron powder diffraction patterns were dramatically reduced (Fig. 5). The corresponding change in the X-ray pattern of Ti$_2$Zr and

Fig. 5. Best fit to the neutron diffraction pattern of alloy Ti$_2$Zr. The observed data points are marked as crosses, and the modelled diffraction pattern is the solid fit to those points. The tick marks underneath the pattern represent peak positions from each phase: the lower set is from the α-phase and, the middle set from the ω-phase, and the upper set marks the positions of the weak peaks from the V can. Top: with O in model. Bottom: without O in model.
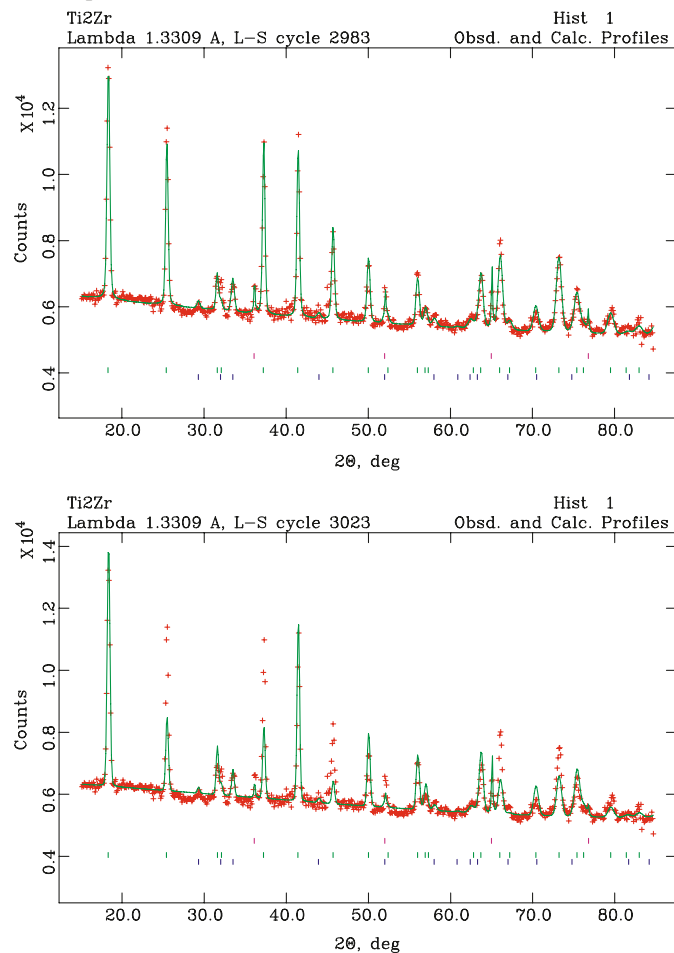
Ti$_2$ZrO$_{0.12}$ is virtually imperceptible: R_p changes from 10.5% to 10.2% (Fig. 4). Tests were performed to see whether the ω-phase was ideal, or if the collapse was only partly complete. Refinement of the ω-phase in $P\bar{3}m1$ gave the $z_0 =$ 0.493(9), so future refinements were done in $P6/mmm$. To verify the O content, LECO measurements were made for a subset of the samples: powdered Ti$_2$Zr, TiZr and the starting material Zr. These gave 12.6, 9.2, and 8.9 atom%, respectively.[4] The $Cmmm$ structure is only achieved by low-temperature annealing [14]. We saw none of the expected additional $Cmmm$ superlattice peaks in the diffraction patterns of our powders that had rapidly cooled from high temperature. Further hydriding cycles revealed that α and ω were completely replaced, principally by tetragonal ThH$_2$ structure-type and the λ-Ti$_2$ZrH$_4$ C15 Laves phase (MgCu$_2$ structure-type), together with free α-ZrO$_2$, as observed in similar systems [43, 44]. Upon dehydriding, the α- and ω-phases reappeared.

---

[4] J. Huot. Personal communication. 2009.

4. Discussion

The potential $\alpha \rightarrow \omega$ transition pathways have been studied by computer simulations [40, 45, 46]. It was concluded that the presence of octahedral interstitials (e.g., C, N, O) strongly inhibited the $\alpha \rightarrow \omega$ pathway [40]. In essence, they increase the activation barrier along the reaction coordinate. As the same barrier is present for the reverse $\omega \rightarrow \alpha$ transition, it appears probable that this reverse transition would be inhibited by the presence of interstitials. On rapid quenching of the SHS samples, the β-state either inverts to α or is trapped in the ω state, to which it can readily fluctuate.

In this case, free oxide in the form of α-ZrO$_2$ was present in the starting materials, but because of the high solubility of O in these metals, reasonable proportions of ω-phase could form, even where no free oxide was present in the starting materials. It seems likely that any observation of ω-phase in Ti-Zr-Hf alloys should be viewed with suspicion as being stabilized by interstitials, most probably O. Oxygen-levels were relatively high in these samples, but it appears very little O may be required to pin the ω-phase. Zr, Ti, and Hf are all very effective O getters. Sass reported an experiment on an alloy formed from zone-refined Zr and Ti quenched in diffusion pump oil from 1000 °C: when the heat treatment was done in Ar, ω-phase was retained, whereas the same heat treatment done in a 5×10^{-5} torr (1 torr = 133.322 4 Pa) vacuum prior to quenching resulted in no ω-formation [47]. In bottled Ar, trace amounts of N$_2$ and O$_2$ remain, and it seems probable that it is the effect of these small amounts of impurities that caused retention of ω [14, 40, 47]. Therefore, it is likely that there is a continuum of structures, from the ω-alloy containing a few octahedral interstitials to Ti$_2$ZrO, so that the structure could be described as a defect, or interstitial, solid solution of O and octahedral vacancies: Ti$_{2-x}$ (Zr,Hf)$_x$O$_y\square_{1-y}$, where y could take a wide variety of values from near zero to 1. A systematic study of the amount of the minimum amount of O required appears to never have been performed. For the annealed stoichiometric Ti$_2$ZrO reported by Déchamps et al. [14], the transition from bcc through the trigonal–hexagonal ω structures to the final $Cmmm$ structure involves progressively further ordering of O from complete disorder over all octahedral sites, to complete order on only 1/9 of them (Table 2), so that this structure is best described as a well-ordered oxide.

5. Conclusions

The ω-phase has been studied for various compositions in the Ti-Zr-Hf concentration triangle. There is no evidence of an ω-phase along the Zr-Hf tie line. We have clarified the mechanism of the phase transition in these ordered ω-phases and shown that the previously proposed 2-step mechanism of site ordering, followed by displacement is probably incorrect, as a simpler single-step mechanism is apparent from examining the group theory behind the transition. There is an error in the ICSD database concerning the orthorhombic, fully O-ordered ω-phase. It is probable that the ω-phase exists all the way from a stoichiometric oxide such as Ti$_2$ZrO to nearly pure alloy, stabilized by very small amounts of in-

Table 3. Site occupancies refined from the ω-phase from joint X-ray and neutron refinements of the two binary Ti-Zr compositions and two ternary compositions of Ti-Zr-Hf refined in $P6/mmm$. For $Ti_{0.66}Zr_{0.22}Hf_{0.12}$, the Hf-content was fixed to zero, since it refined to zero within one esd. The compositions listed are the nominal compositions of the bulk powder, which is partitioned over the ω- and α-phases.

		TiZr	Ti$_2$Zr	Ti$_{0.33}$Zr$_{0.33}$Hf$_{0.33}$	Ti$_{0.66}$Zr$_{0.22}$Hf$_{0.12}$
	a(Å)	4.8640(7)	4.8025(2)	4.8428(14)	4.7962(2)
	c(Å)	3.0465(5)	3.0112(2)	3.0191(16)	3.0008(2)
1a	Zr	0.938(17)	0.781(2)	0.706(18)	0.951(6)
	Ti	0.062(17)	0.219(2)	0.042(11)	0.049(5)
	Hf			0.252(15)	
2d	Zr	0.328(2)	0.188(1)	0.256(15)	0.079(6)
	Ti	0.672(2)	0.812(1)	0.713(10)	0.921(5)
	Hf			0.027(18)	
3f	O	0.143(5)	0.143(2)	0.10(11)	0.080(11)

terstitials [47]. Therefore, the appearance of any ω phase at ambient (T,P) in the X-ray powder diffraction of Ti-Zr-Hf alloys may be a sign of contamination, probably by O, as X-ray powder diffraction of alloys containing even 10 atom% O can barely distinguish alloy from oxide.

Acknowledgments

References

1. S.K. Dolukhanyan, V.Sh. Shekhtman, A.G. Aleksanyan, O.P. Ter-Galstyan, and G.Ye. Abrosimova, and M.K. Sakharov. Zhurnal Chim. Phys. **26**, 36 (2007).

2. A.G. Aleksanyan, S.K. Dolukhanyan, A.A. Mantashyan, D.G. Mailyan, O.P. Ter-Galstyan, and V.Sh. Shekhtman. New technique for producing the alloys based on transition metals. NATO Science Series, ICHMS 2007. *In* Carbon Nanomaterials in Clean Energy Hydrogen Systems. *Edited by* B. Baranovski et al. Springer. 2008. p. 783.

3. A.G. Aleksanyan, D.G. Mailyan, S.K. Dolukhanyan, V.Sh. Shekhtman, and O.P. Ter-Galstyan. Alternativnaya Energetika i Ekologia, **9**, 22 (2008).

4. S.K. Dolukhanyan, A.G. Aleksanyan, O.P. Ter-Galstyan, D.G. Mailyan, V.Sh. Shekhtman, M.K. Sakharov, and S.S. Khasanov. The peculiarities of formation of alloys structure in the system Ti-Zr-Hf-H. NATO Science Series, ICHMS 2007. *In* Carbon Nanomaterials in Clean Energy Hydrogen Systems. *Edited by* B. Baranovski et al. Springer. 2008. p. 733.

5. S.K. Dolukhanyan, A.G. Aleksanyan, O.P. Ter-Galstyan, V.Sh. Shekhtman, M.K. Sakharov, and G.E. Abrosimova. Russ. J. Phys. Chem. **2**, 563 (2007).

6. I.P. Swainson. Neutron transmission investigation of metal hydrides for use in neutron shielding. National Research Council of Canada Report: CNBC-2009–1. 2009.

7. S.K. Dolukhanyan, M.D. Nersisyan, A.B. Nalbandyan, I.P. Borovinskaya, and A.G. Merzhanov. Proc. Acad. Sci. USSR, **231**, 675 (1976).

8. S.K. Dolukhanyan. J. Alloy. Comp. **253–254**, 10 (1997). doi:10.1016/S0925-8388(96)03071-X.

9. S.K. Dolukhanyan, H.G. Hakobyan, and A.G. Aleksanyan. Int. J. SHS, **1**, 530 (1992).

10. M. Miyake, M. Uno, and S. Yamanaka. J. Nucl. Mater. **270**, 233 (1999). doi:10.1016/S0022-3115(98)00779-X.

11. V.A. Lavrenko, V.Zh. Shemet, L.A. Petrov, O.A. Teplov, and S.K. Dolukhanyan. Oxid. Met. **33**, 177 (1990). doi:10.1007/BF00665675.

12. V.N. Fokin, Yu.I. Malov, E.E. Fokina, and S.L. Troitskaya. Int. J. Hydrogen Energy, **20**, 387 (1995). doi:10.1016/0360-3199(94)00075-B.

13. A. Dubertret and M. Fayard. J. Phys. (Paris), **38**, C7 (1977). doi:10.1051/jphyscol:1977791.

14. M. Déchamps, P. Lehr, A. Dubertret, and M. Fayard. Mater. Res. Bull. **7**, 1369 (1972). doi:10.1016/0025-5408(72)90173-0.

15. J.C. Jamieson. Science, **140**, 72 (1963). doi:10.1126/science.140.3562.72. PMID:17746009.

16. E. Tonkov. High pressure phase transformations. Philadelphia: Gordon and Breach. Vol. 2. 1992. pp. 682–691.

17. I.O. Bashkin, A.Yu. Pagnuev, A.F. Gurov, V.K. Fedotov, and G.Ye. Abrosimova, and Ye.G. Poniatovskiy. J. Phys. C: Solid State Phys. **42**, 163 (2000).

18. W. Petry, A. Heiming, J. Trampenau, M. Alba, C. Herzig, H.R. Schober, and G. Vogl. Phys. Rev. B, **43**, 10933 (1991). doi:10.1103/PhysRevB.43.10933.

19. A. Heiming, W. Petry, J. Trampenau, M. Alba, C. Herzig, H.R. Schober, and G. Vogl. Phys. Rev. B, **43**, 10948 (1991). doi:10.1103/PhysRevB.43.10948.

20. Y. Noda, Y. Yamada, and S.M. Shapiro. Phys. Rev. B, **40**, 5995 (1989). doi:10.1103/PhysRevB.40.5995.

21. A. Heiming, W. Petry, J. Trampenau, M. Alba, C. Herzig, and G. Vogl. Phys. Rev. B, **40**, 11425 (1989). doi:10.1103/PhysRevB.40.11425.

22. R.F. Domagala, S.R. Lyon, and R. Ruh. J. Am. Ceram. Soc. **56**, 584 (1973). doi:10.1111/j.1151-2916.1973.tb12421.x.

23. L. Fykin, V. Glazova, and I. Kornilov. Dokl. Akad. Nauk SSSR, **182**, 576 (1968).

24. L.E. Fykin, V.V. Vavilova, I.I. Kornilov, R.P. Ozerov, and S.P. Solov'ev. Dokl. Akad. Nauk SSSR, **194**, 1374 (1970).

25. K.-L. Lin and C.-C. Lin. J. Am. Ceram. Soc. **88**, 1268 (2005). doi:10.1111/j.1551-2916.2005.00218.x.

26. K.-L. Lin and C.-C. Lin. J. Am. Ceram. Soc. **89**, 1400 (2006). doi:10.1111/j.1551-2916.2005.00877.x.

27. H.T. Stokes, D.M. Hatch, and B.J. Campbell. ISOTROPY, stokes.byu.edu/isotropy.html. 2007.

28. B.J. Campbell, H.T. Stokes, D.E. Tanner, and D.M. Hatch. J. Appl. Cryst. **39**, 607 (2006). doi:10.1107/S0021889806014075.

29. S. Miller and W.F. Love. Tables of Irreducible Representations of Space Groups and Co-Representations of Magnetic Space Groups. Pruett, Boulder, Co, USA. 1967.

30. S.A. Spachner. Trans. Metall. Soc. AIME, **212**, 57 (1958).

31. A.E. Austin and I.R. Doig. Trans. AIME, **209**, 27 (1957).

32. E.U. Lee. J. Appl. Cryst. **3**, 413 (1970). doi:10.1107/S0021889870006581.

33. V.P. Dmitriev, S.P. Rochal, Y.M. Gufan, P. Tolédano, and A.F. Williams. *In* Phase Transformations '87, Cambridge, UK, 6–10 July 1987. 1988. pp. 430–432.

34. J.C. Tolédano and P. Tolédano. World Scientific Lecture Notes in Physics, **3**, 202 (1987).

35. H.E. Cook. Acta Metall. **23**, 1027 (1975). doi:10.1016/0001-6160(75)90107-8.

36. H.E. Cook. Acta Metall. **23**, 1041 (1975). doi:10.1016/0001-6160(75)90108-X.

37. H.E. Cook. Acta Metall. **22**, 239 (1974). doi:10.1016/0001-6160(74)90014-5.

38. T. Fukunaga, S. Shibuya, K. Suzuki, and M. Misawa. J. Mater. Sci. Lett. **6**, 1435 (1987). doi:10.1007/BF01689313.

39. U. Köhler and Ch. Herzig. Phys. Status Solidi B, **144**, 243 (1987). doi:10.1002/pssb.2221440122.

40. R.G. Hennig, D.R. Trinkle, J. Bouchet, S.G. Srinivasan, R.C. Albers, and J.W. Wilkins. Nat. Mater. **4**, 129 (2005). doi:10.1038/nmat1292. PMID:15665839.

41. V.F. Sears. Scattering lengths for neutrons. *In* International Tables for Crystallography. Vol. C. 2006. p. 444.

42. V.F. Sears. Neutron News, **3**, 26 (1992). doi:10.1080/10448639208218770.

43. J. Huot, E. Akiba, and H. Iba. J. Alloy. Comp. **228**, 181 (1995). doi:10.1016/0925-8388(95)01884-0.

44. Y. Tokaychuk, L. Keller, and K. Yvon. J. Alloy. Comp. **394**, 126 (2005). doi:10.1016/j.jallcom.2004.11.018.

45. D.R. Trinkle, R.G. Hennig, S.G. Srinivasan, D.M. Hatch, M.D. Jones, H.T. Stokes, R.C. Albers, and J.W. Wilkins. Phys. Rev. Lett. **91**, 025701 (2003). doi:10.1103/PhysRevLett.91.025701. PMID:12906490.

46. D.R. Trinkle, D.M. Hatch, H.T. Stokes, R.G. Hennig, and R.C. Albers. Phys. Rev. B, **72**, 014105 (2005). doi:10.1103/PhysRevB.72.014105.

47. S.L. Sass. Acta Metall. **17**, 813 (1969). doi:10.1016/0001-6160(69)90100-X.